Chemical Science

ROYAL SOCIETY OF CHEMISTRY

EDGE ARTICLE

View Article Online
View Journal

Cite this: DOI: 10.1039/d6sc02312f

All publication charges for this article have been paid for by the Royal Society of Chemistry

Beyond the two-conformer model: boat conformers provide stereoselectivity in S_N1-type glycosylations of *manno*-type donors

Wouter A. Remmerswaal, †[a] Daan Hoogers, †[a] Joeri Schoenmakers, [a] F. Matthias Bickelhaupt, [bcd] Thomas Hansen *[b] and Jeroen D. C. Codée *[a]

Received 20th March 2026
Accepted 13th April 2026

DOI: 10.1039/d6sc02312f

rsc.li/chemical-science

Oxocarbenium ions play a central role in shaping the stereochemical outcome of S_N1-type glycosylation reactions. Generally, glycosylations involving $^4H_3$-like glycosyl cations proceed with α-selectivity, whereas those involving $^3H_4$-like cations furnish β-products, reflecting favorable chair-like transition states. While this analysis holds for many glycosyl cations, it breaks down for mannosyl donors. Although the mannosyl $^3H_4$ cation is significantly more stable than its $^4H_3$ counterpart, addition of weak carbon nucleophiles predominantly yields α-products. To elucidate the origin of this deviation from the predictive two-conformer model, we examined *C*-allylation reactions of nucleophiles spanning three orders of magnitude in reactivity with a series of glucosyl and mannosyl-type donors (mannose, rhamnose, and mannuronic acid). Quantum chemical calculations of the competing reaction pathways show that, for mannose, glycosylation proceeds under Curtin–Hammett control *via* α-attack on a $B_{2,5}$-like (boat) oxocarbenium ion through an $^OS_2$-type transition state that avoids the severe steric (Pauli) repulsion present along the β-$^1C_4$ trajectory. Activation-strain and energy-decomposition analyses quantify the steric and electronic effects and explain why rhamnose, with reduced C6 steric demand, provides slightly more β-selective glycosylation reactions and mannuronic acid, of which the $^3H_4$ is exceptionally favorable, shows β-selectivity. The mechanistic framework provides a quantitative basis for understanding and designing stereoselective S_N1-type glycosylations.

Introduction

The structure of oxocarbenium ions plays a central role in shaping the stereochemical outcome of glycosylation reactions.[4–8] These intermediates typically arise in S_N1-type substitution reactions, where ionization and expulsion of the leaving group is the rate-determining step, to generate a short-lived, oxocarbenium ion that subsequently undergoes nucleophilic attack. Despite the high reactivity of these intermediates, and the fact that nucleophilic addition occurs after the rate-determining step, they can display striking stereoselectivity.[9–13]

The fleeting nature of oxocarbenium ions makes them difficult to study directly, complicating the establishment of clear structure–reactivity–stereoselectivity relationships.[14,15] They have been studied in super-acid media, in which their lifetime is extended to allow NMR spectroscopic structural analysis,[16,17] and *in vacuo* using IR techniques.[18–22] Their involvement in glycosylation reactions has also been shown using kinetic isotope effect measurements[23–25] and cation clock experiments.[26] Quantum chemical calculations have been instrumental in providing insight into the stereoelectronic effects of the ring substituents on the structure, stability, and reactivity of these ions.[27–34]

In glycosylation reactions proceeding through an oxocarbenium ion intermediate, the stereochemical outcome can be rationalized by the two-conformer model (see Fig. 1A).[35,36] This model proposes that oxocarbenium ions typically adopt one of two half-chair conformations ($^3H_4$ or $^4H_3$) each leading to a preferred product *via* a chair-like transition state.[37,38] The model argues that $^3H_4$-like ions will undergo top-face attack to give the β-anomer, while $^4H_3$-like ions undergo bottom-face attack to give the α-anomer. This relationship has been validated for many systems.[34] Woerpel and co-workers have systematically mapped the effect of (electron withdrawing) ring substituents on the stability and reactivity of the half chair conformations and shown that the ground state conformational preference of the ions can be an all-important factor in shaping the stereochemical outcome of addition reactions on these

[a]*Leiden University, Leiden Institute of Chemistry, Einsteinweg 55, 2333 CC Leiden, The Netherlands. E-mail: jcodee@chem.leidenuniv.nl*

[b]*Department of Chemistry and Pharmaceutical Sciences, Amsterdam Institute of Molecular and Life Sciences (AIMMS), Vrije Universiteit Amsterdam, De Boelelaan 1108, 1081 HZ Amsterdam, The Netherlands*

[c]*Institute for Molecules and Materials, Radboud University, Heyendaalseweg 135, 6525 AJ Nijmegen, The Netherlands*

[d]*Department of Chemical Sciences, University of Johannesburg, Auckland Park, Johannesburg 2006, South Africa*

† These authors contributed equally.

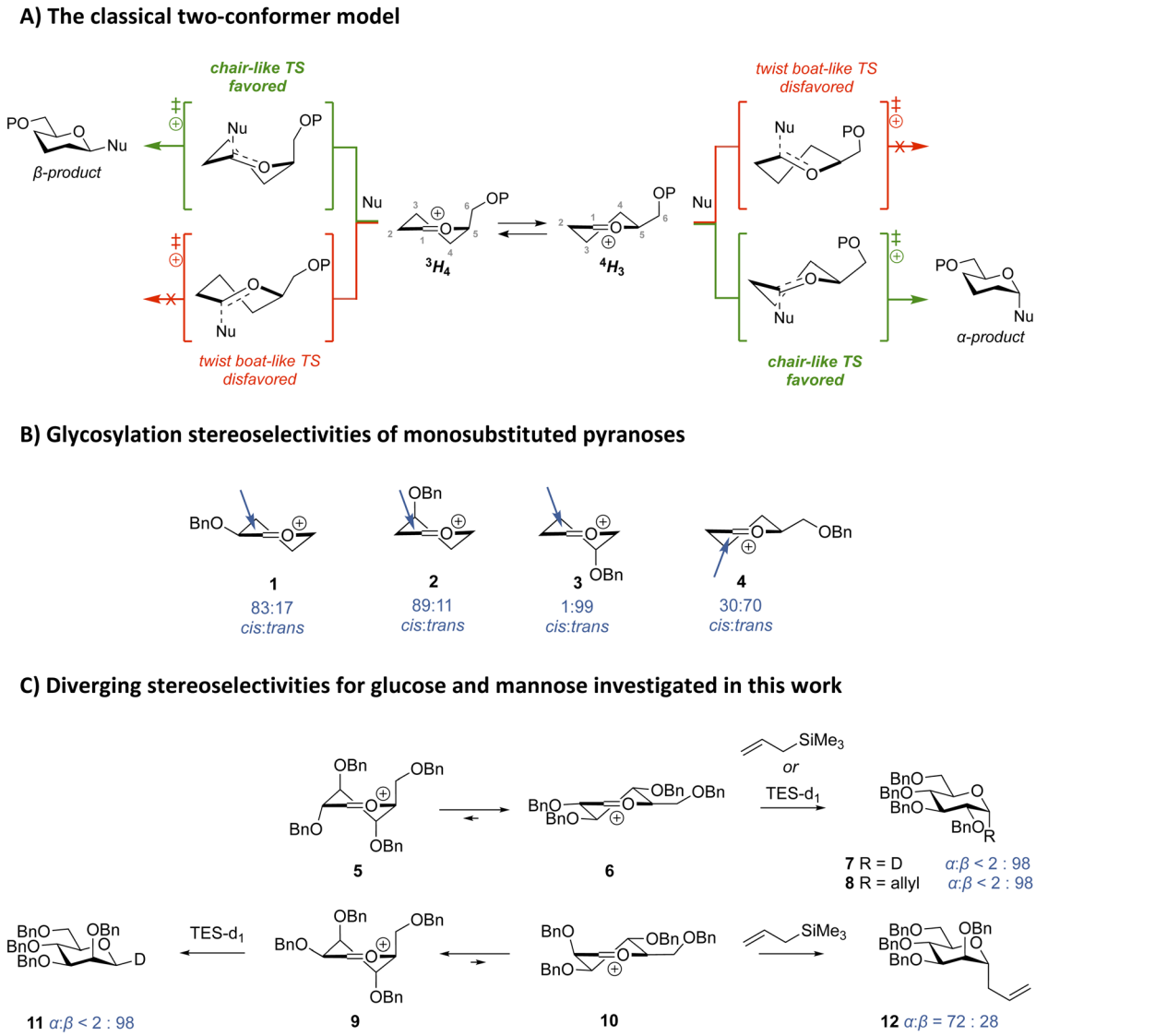

Fig. 1 (A) The two-conformer model for understanding and predicting the stereoselectivity of glycosyl cations. P = protecting group. (B) Stereoselectivities of S_E2' glycosylation reactions with monosubstituted pyranosyl donors performed by Woerpel and co-workers. (C) The diverging stereoselectivities of the glycosylation reactions of the glucosyl and mannosyl cations with TES-d_1 and allyltrimethylsilane investigated in this work.

ions.[39–43] They showed that alkoxy substituents at C3 and C4 are most stabilizing/least destabilizing when positioned in a pseudo-axial orientation, while alkoxy -groups at C2 are placed preferentially in a pseudo-equatorial position to allow hyperconjugative stabilization of the oxocarbenium ion by the axial C2–H2 bond.[44] On steric grounds, the C5 substituent prefers a pseudo-equatorial orientation.[45] These orientational preferences can translate to highly stereoselective addition reactions (Fig. 1B), with the 3-*O*-benzyl substituted pyranosyl ion **2** stereoselectively delivering 1,3-*cis* addition products, while the 4-*O*-benzyl regioisomer **3** can give exclusively 1,4-*trans* products and a 2-*O*-benzyl substituent (as in **1**) steers the addition reactions to favor the 1,2-*cis* products. In contrast to its conformational preference, the presence of a single C-5 alkoxymethyl group (as in **4**) provides only modest selectivity towards the formation of the 1,5-*trans* product, highlighting the subtleties involved even in simple systems.[39]

When multiple substituents are present their effects can be mutually supportive, or they can counteract one another. To gauge the overall effect of the complete substitution pattern, we have previously developed computational methods to study the structure and stability of fully substituted glycosyl oxocarbenium ions and mapped how the ring substituents affect the overall shape of the ions,[34,46] and methodologies to compare the addition reactions.[47] The striking *cis*-selectivity in addition reactions to many pyranosyl oxocarbenium ions could be explained from the ground state preference of the involved ions. For example, for the glucosyl ion the $^4H_3$ ion **6** was found to be the most favorable oxocarbenium ion conformer, and addition reaction of triethylsilane-*d* (TES-d_1) provided the 1,2-*cis* (α) product **7** with exclusive stereoselectivity (Fig. 1C). The addition

reaction of TES-d_1 to the mannosyl cation, which preferentially takes up a $^3H_4$ conformation (**9**), also proceeds with exclusive 1,2-*cis*-stereoselectivity to deliver the β-product **11** (Fig. 1C).[34]

However, the nature and reactivity of the nucleophile can have a strong effect on the stereochemical course of the addition reactions. When weaker and/or more sterically demanding nucleophiles are used, the stereoselectivity of the addition reactions can change because interactions between the incoming nucleophile and oxocarbenium ion become important. The mannosyl oxocarbenium ion presents a prominent example: where the addition of TES-d_1 stereoselectively provides the β-product, the corresponding *C*-allyl mannoside **12** is formed with (moderate) α-selectivity when allyltrimethylsilane is used as a nucleophile.[45]

Woerpel and co-workers have proposed that the erosion of stereoselectivity in this case is caused by the steric interactions of the incoming nucleophile and the most stable $^3H_4$ mannosyl oxocarbenium ion **9**. By invoking a Curtin–Hammett kinetic scenario, they reasoned that the major α-product is formed from the least populated $^4H_3$ conformer **10**, which is in rapid equilibrium with its more stable $^3H_4$ counterpart. This change in stereoselectivity is not observed for the glucosyl ion, because the incoming nucleophile does not encounter prohibitively large steric interactions on the α-face of the $^3H_4$ ion **6**.

To unravel the origin behind the diverging reaction outcomes and understand why and when different Curtin–Hammett scenarios come into play in addition reactions of the mannosyl oxocarbenium ion – and by extension other glycosyl cations – we have investigated a systematic set of *C*-allylation reactions in which we have paired different allyl nucleophiles of gradually changing reactivity with gluco- and *manno*-configured donors. To understand the stereoelectronic effects that shape the Curtin–Hammett kinetic scenario in the addition reactions to the mannose oxocarbenium ion, we have probed mannosyl, rhamnosyl and mannuronic acid systems. These have revealed clear reactivity-stereoselectivity trends. We have employed quantum chemical calculations, including potential energy surface (PES) mapping and activation strain model (ASM) analyses, to investigate the different reaction paths. These studies have identified an unexpected low-energy pathway for the addition reactions to the mannosyl cation. The steric interactions in the transition state of the addition reaction taking place on the β-face of the $^3H_4$ mannosyl cation and relatively high energy of the $^4H_3$ intermediate make that an alternative pathway, involving α-attack on a boat-like ($B_{2,5}$) intermediate, becomes most favorable. Our ASM analyses have quantified the steric and electronic effects in the different transition states, providing quantitative insight into how they steer the reaction outcome.

Results and discussion

Model glycosylation reactions

To investigate the different addition pathways on glycosyl oxocarbenium ions, we examined glucosyl and mannosyl donors **13** and **14** (Table 1). Each of these was reacted with a series of allyl nucleophiles of similar size but spanning three orders of magnitude in nucleophilicity: allyl (chloro)dimethylsilane (N = −0.57), allyltrimethylsilane (N = 1.68), and allyltributylstannane (N = 5.45).[48–50] The results of these *C*-allylation reactions are summarized in Table 1. The glucosyl donor **13** predominantly delivered the α-products with all nucleophiles

Table 1 Model *C*-glycosylation reaction results from glucosyl donor, **13**, and mannosyl donor, **14**. The stereoselectivity of the reaction is expressed as α : β and based on ^{1}H-NMR of purified α/β-product mixtures. Pre-activation-based glycosylation conditions were used: donor **13** or **14** (1.0 eq.), Tf_2O (1.3 eq.), Ph_2SO (1.3 eq.), TTBP (2.5 eq.), DCM (0.05 M), −80 to −60 °C, then add nucleophile (2.0 eq.) at −80 °C and allow to warm to −60 °C[1]

		$SiMe_2Cl$	$SiMe_3$	$SnBu_3$
		A	**B**	**C**
	N	-0.45	1.79	4.41
	Donor	α:β (yield)	α:β (yield)	α:β (yield)
13	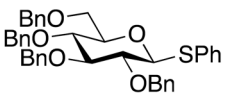	**13A** >98:2 (32%)	**13B** >98:2 (41%)	**13D** 69:31 (70%)
14	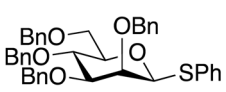	**14A** >98:2 (23%)	**14B** 72:28 (66%)	**14D** 28:72 (69%)

>90:10	>75:25	>60:40	50:50	<40:60	<25:75	<10:90

tested. The erosion of α-selectivity observed with allyltributylstannane may be accounted for by the higher reactivity of this nucleophile, making direct substitution of the intermediate α-triflate through a more associative S_N2-like transition state possible. The stereoselectivity of the reactions of the mannosyl donor **18** exhibited a much larger dependence on nucleophile reactivity. The reaction with the weakest allyl nucleophile, showed complete α-selectivity (α : β > 98 : 2), which shifted to a moderate α-selectivity (α : β = 72 : 28) for allyltrimethylsilane (in line with reports by Crich[51]), to a moderately β-selective reaction (28 : 72) for the strongest nucleophile (in line with reports by McGarvey[52]). The results for the weaker nucleophiles, allyl (chloro)dimethylsilane and allyltrimethylsilane, may be accounted for by Woepel's hypothesis that the α-products are formed from the minor $^4H_3$-like oxocarbenium ion (**10**), that is in equilibrium with its more stable $^3H_4$-counterpart (**9**). In the chair-like transition state originating from the $^3H_4$-oxocarbenium ion, steric interactions will develop with the pseudo-axial substituents at C3 and C5. With weaker nucleophiles, that react through a later transition state these interactions will be more severe, making this transition state less favorable. The higher α-selectivity for the weakest nucleophile (allyl (chloro)dimethylsilane) in comparison with allyltrimethylsilane is in line with this hypothesis. An earlier transition state for allyltributylstannane, (partially) restores the β-selectivity, predicted by the two-conformer model. A more associative pathway, in which the anomeric α-triflate (or contact ion pair) is substituted by the nucleophile can also contribute to the 1,2-*cis* selectivity.

Computational analysis

To better rationalize these experimental observations, we computed potential energy surfaces for these addition reactions in DCM solution at the PCM(CH_2Cl_2)-B3LYP/6-311G (d,p) level of theory. Benzyl groups were replaced with methyl ethers to reduce computational cost. In several cases, the electronic potential energy surface for reactions with these cationic species appeared barrierless. However, entropic contributions often introduced an overall reaction barrier. To identify the corresponding barriers, we performed constrained scans along the reaction coordinate and evaluated partition functions at each computed point to obtain Gibbs free energies. This approach was benchmarked against systems for which both constrained and unconstrained reaction barrier were available (see SI for all computational details) and was found to reproduce consistent trends.

For the most nucleophilic allylic reagents, such as allyltributylstannane, we were unable to locate transition states on the electronic potential energy surface. As discussed above, the high reactivity of these nucleophiles leads to barrierless additions. Because the strongest deviation from the stereoselectivity predicted by the two-conformer model was found in the additions of allyl (chloro)dimethylsilane, and this nucleophile also allowed for the location of most transition states, these will be used in the following analyses and discussion. For each donor-nucleophile pair, multiple plausible trajectories were identified: α-attack *via* a chair-like $^4C_1$ from a $^4H_3$, a $^3S_1$ from a $^3H_4$, or an $^OS_2$ from a boat-like $B_{2,5}$; and β-attack *via* a $^1C_4$ from a $^3H_4$, a $^1S_3$ from a $^4H_3$, or a $^1S_5$ from a $B_{2,5}$ (Fig. 2A). Fig. 2B compares the barrier heights for the addition reactions of allyl (chloro)dimethylsilane on the glucosyl and mannosyl cations. The $\Delta\Delta G^\ddagger$ values of −1.6 kcal mol^{-1} (glucose) and −2.2 kcal mol^{-1} (mannose) between the lowest α- and β-forming transition states are fully consistent with the experimentally observed >98 : 2 α-selectivities for allyl (chloro)dimethylsilane: application of the Eyring equation at −60 °C (213 K) gives predicted α : β ratios of *ca.* 98 : 2 and 99.5 : 0.5, respectively.

For the glucosyl cation, the lowest transition state (the $^4C_1$-like TS, $\Delta G = 11.2$ kcal mol^{-1}) originated from the lowest energy oxocarbenium ion half chair (the $^4H_3$-ion **6**), in keeping with the two-conformer model. As previously established, the latter half chair is more stable than its counterpart on the other side of the Cremer-Pople conformational sphere, which adopts a the $E_4/^2S_O$ -like structure. This conformer deviates from the canonical $^3H_4$ conformation (**5**, shown in Fig. 1) to diminish the steric interactions between all the pseudo-axial substituents in this half chair conformation. These steric interactions also make the transition states departing from this conformer unfavorable. As a result, attack of the nucleophile on the β-face of the lowest energy $^4H_3$ ion, which deforms the glucosyl cation into a $^1S_3$-like structure in the transition state, represents the lowest energy pathway to the β-products, being more favorable than the chair-like transition state originating from the $E_4/^2S_O$ -like ion.

The mannosyl $^3H_4$ cation **9** is significantly more favorable than its $^4H_3$ counterpart **10** (by 2.4 kcal mol^{-1}). However, the trajectory of the incoming nucleophile on the β-face of the former ion (see Fig. 2C, mannose-TS-β-$^1C_4$), is met with significant steric interactions, which makes this pathway rather unfavorable (13.0 kcal mol^{-1}). The chair-like transition state originating from the alternative, higher energy $^4H_3$ half-chair oxocarbenium ion **10** was found to be more favorable (12.5 kcal mol^{-1}). Notably the most favorable approach we located, involved attack of allyl (chloro)dimethylsilane on the α-face of the $B_{2,5}$ conformer of mannose. In this mode of attack the mannose ring adopts a $^OS_2$-like conformation, thereby avoiding severe steric interactions between the nucleophile and pseudo-axial C3 and C5 substituents, which destabilize the β-$^1C_4$ approach (see Fig. 2C, mannose-TS-α-$^OS_2$). Notably, Crich and co-workers have previously described a similar transition state conformation for the intramolecular attack of an C2-trimethylsilyl (methallyl) ether in a benzylidene mannose system.[22] We could also find a transition state for the attack of the nucleophile on the β-face of the $B_{2,5}$ mannosyl ion, but this was found to be significantly less favorable (13.4 kcal mol^{-1}).

While the potential energy surfaces and transition state barriers discussed above are reported as Gibbs free energies (ΔG), we verified that the relative reactivity trends are identical when considering the corresponding electronic energies (ΔE). Accordingly, the selectivity trends observed in the PES analysis can be rationalized using the activation strain model (ASM) of reactivity and energy decomposition analysis (EDA), which describe the reaction profile in terms of electronic energies.[53–56] In this fragment-based approach, the potential energy surface can be described with respect to, and understood in terms of,

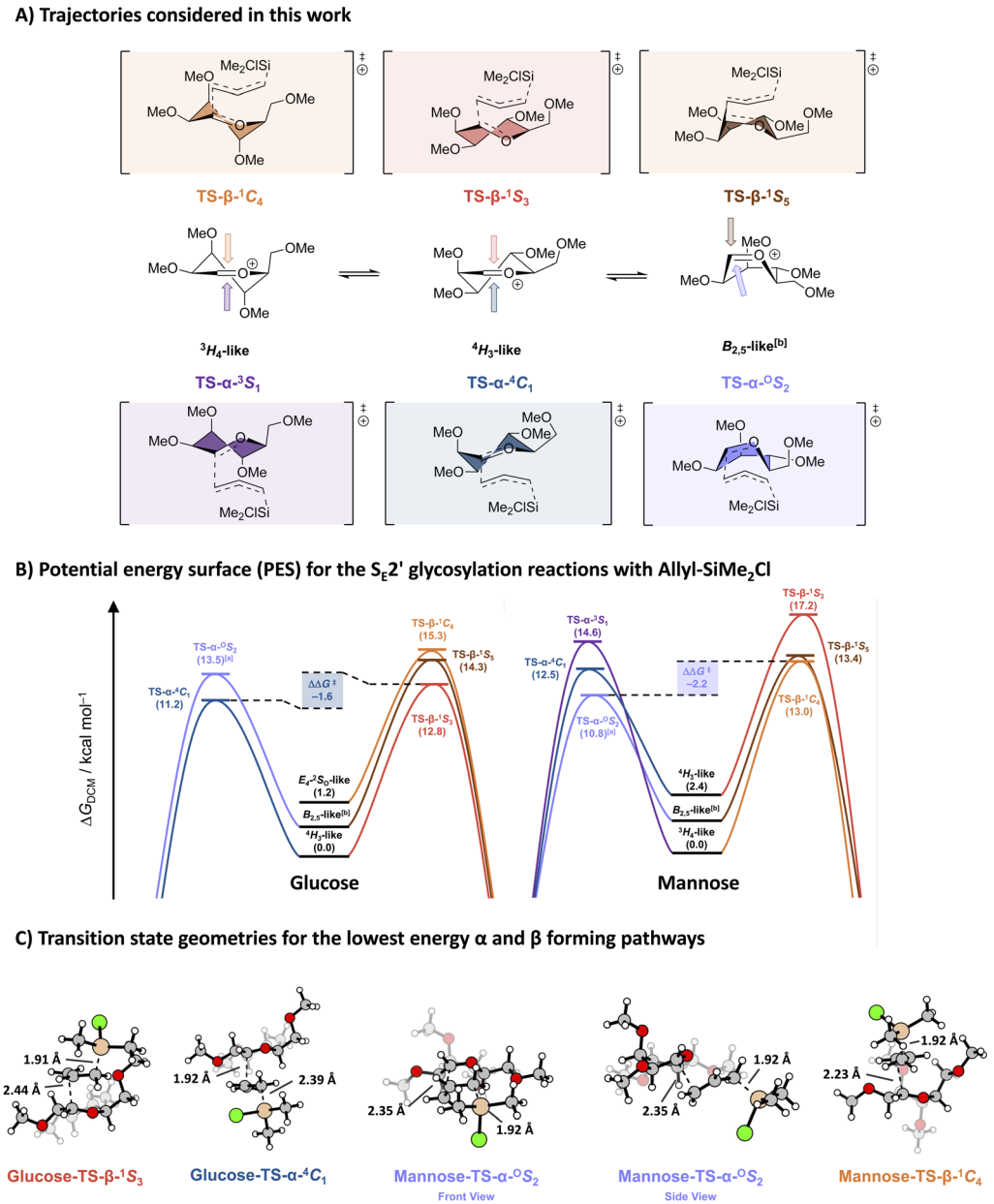

Fig. 2 (A) An overview of the possible S_E2' reaction trajectories considered in this work, and (B) the corresponding reaction profiles of the addition of allyl (chloro)dimethylsilane to the glucosyl and mannosyl cations *via* the following transition states: TS-β-$^1C_4$ (orange), TS-β-$^1S_5$ (brown), TS-β-$^1S_3$ (red), TS-α-$^OS_2$ (light violet), TS-α-$^4C_1$ (blue), and TS-α-$^3S_1$ (purple). Energies are depicted as Gibbs free energies ($T = 213.15$ K) and were computed at PCM(CH_2Cl_2)-B3LYP/6-311G (d,p). The TS-α-$^3S_1$ on glucose is unfavourable and could not be located. [a]A representative structure for the transition state geometry was used.[2] [b]The itinerary leading up to TS-α-$^OS_2$ and TS-β-$^1S_5$ start from a boat-like non-stationary point. (C) Structures of the lowest energy transition states of the S_E2' reactions of ally (chloro)dimethylsilane with the glucosyl or mannosyl cations leading to the α and β products. The mannose-TS-α-$^OS_2$ is depicted from two distinct angles to show the 'sideways' approach of the nucleophile, avoiding most steric interaction.

the characteristics of the reactants, here the allylic nucleophile and the glycosyl oxocarbenium ion substrate. The energy (ΔE) along the potential energy surface is expressed as the sum of the strain energy (ΔE_{strain}) required to deform the individual reactants from their equilibrium geometries and the interaction energy (ΔE_{int}) between the deformed fragments: $\Delta E = \Delta E_{strain} + \Delta E_{int}$. These are then plotted along the potential energy surfaces in activation strain diagrams (ASDs). Here, the glycosyl oxocarbenium ion and the allylic *C*-nucleophile served as the two fragments. The intrinsic reaction coordinate (IRC) was projected onto the carbon-leaving group (C···Si) distance of the nucleophile, which changes in a well-defined manner during the S_E2' attack, and this coordinate has been validated as a suitable reaction coordinate for this type of bimolecular processes.[47]

Energy decomposition analysis (EDA) was applied to the ΔE_{int} term to dissect it into the electrostatic interactions (ΔV_{elstat}), Pauli repulsion (ΔE_{Pauli}), and orbital interaction

energy (ΔE_{oi}). EDA values are reported as gas-phase electronic energies (ΔE_{gas}).[57] For consistent comparison, ASM and EDA profiles for different pathways were analyzed at points with identical C···Si distances. Because the EDA terms are highly dependent on the distance between the fragments,[55,56,58,59] we additionally verified the results using double-consistent geometries (DCGs) in which both the C···Si and C1···C-allyl distances were matched (see SI for computational details). This eliminates geometric artefacts that can distort interaction terms, especially the Pauli repulsion term. All DCG-verified data, including geometries and numerical values, are provided in SI Fig. S5 and S6.

Our activation strain analyses revealed that, for mannose, the β-$^1C_4$ pathway accumulates strain more steeply along the C···Si coordinate than the competing α-$^OS_2$ pathway (Fig. 3A, orange). This reflects the deformation required for the $^3H_4$ conformer to accommodate the nucleophilic approach on the β-face, which brings the incoming nucleophile into close proximity with pseudo-axial C3 and C5 substituents. Steric congestion initially manifests as Pauli repulsion (as evident from the corresponding EDA term), part of which is converted into strain upon deformation. Although this strain remains destabilizing, it is less unfavorable than the scenario without deformation, in which Pauli repulsion would increase even more strongly. In

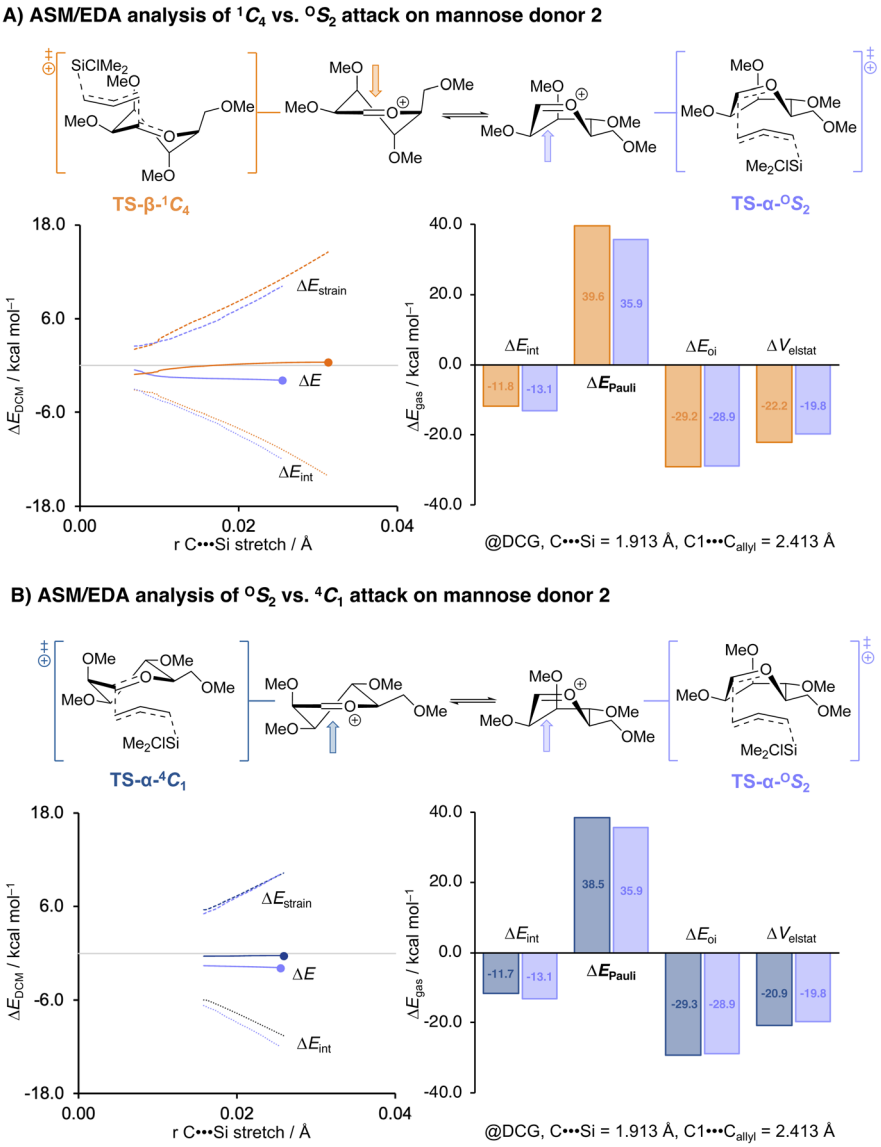

Fig. 3 Activation strain and energy decomposition analyses for the S_E2' reactions of allyl (chloro)dimethylsilane and the mannosyl cation (A) *via* the β-product-forming TS-β-$^1C_4$ (orange) and the α-product-forming TS-α-$^OS_2$ (light violet) and (B) *via* both α-product-forming TS-α-$^4C_1$ (blue) and TS-α-$^OS_2$ (light violet). ASM energy values are plotted to the transition state (indicated by a dot), along the IRC projected on the C···Si bond stretch. EDA results are numerical experiments at double consistent TS-like geometries (ΔE*) obtained from the IRC at a C···Si bond stretch of 1.913 Å. The C1···C_{allyl} were set to 2.413 Å (C···Si and C1···C_{allyl} distances in the consistent TS-like geometry for TS-α-$^4C_1$). Energies are depicted as electronic energies and were computed at PCM(CH_2Cl_2)-B3LYP/6-311G (d,p) for ΔE_{DCM} or ZORA-B3LYP/TZ2P//PCM(CH_2Cl_2)-B3LYP/6-311G (d,p) for ΔE_{gas}.[3]

contrast, while the α-$^{O}S_2$ pathway (light violet in Fig. 3A) starts from a higher-energy $B_{2,5}$ conformer it avoids the most severe steric interactions, which results both in less strain build-up along the reaction trajectory, and less Pauli repulsion from the start of the nucleophilic approach.

Crucially, this mechanistic option is viable because the $^{3}H_4$ and $B_{2,5}$ conformers of the mannosyl cation are relatively close in energy. The small energy gap between these means that the additional strain required to reach the $B_{2,5}$ geometry is not prohibitive under Curtin–Hammett control. Were the $^{3}H_4$-$B_{2,5}$ gap appreciably larger, the cost of conformer interconversion would outweigh the gain in interaction energy in the $^{O}S_2$ transition state and the canonical β-$^{1}C_4$ pathway would be expected to be dominant. Thus, the combination of strong Pauli repulsion for β-attack on the $^{3}H_4$ conformer and a narrow $^{3}H_4/B_{2,5}$ energy gap enables the boat-like itinerary to prevail over the classical two-conformer model.

Finally, it was examined why the bottom-face attack on a boat-like conformation leading to TS-α-$^{O}S_2$ is more favorable than the canonical bottom-face attack on a half chair-like conformation (TS-α-$^{4}C_1$). The ASM analyses are depicted in Fig. 3B, which show the ASDs for these TS-α-$^{4}C_1$ (blue) *versus* the TS-α-$^{O}S_2$ (light violet) pathways. From the C···Si bond stretch diagram, it can be seen that both bottom face pathways incur similar strain, while the approach leading to TS-α-$^{4}C_1$ is paired with less stabilizing interaction energy. The increased destabilizing Pauli repulsion for the TS-α-$^{4}C_1$ pathway is the main contributor to the observed difference in interaction energy. While this might seem counterintuitive, this indicates that at the same $C_1\cdots C_{allyl}$ bond distance, the nucleophile is positioned more favorably in the TS-α-$^{O}S_2$ pathway, than in the TS-α-$^{4}C_1$. Inspection of the structures in Fig. 2, reveals that the terminal allyl methylene group is positioned under the mannose ring in the TS-α-$^{4}C_1$ while it approaches the cation parallel to the C=O^{+} moiety in the TS-α-$^{O}S_2$ avoiding steric interactions with the electrophile.

C6-modified donors

To further test the relative importance of the Pauli repulsion on the β-face and the energy gap between the competing $^{3}H_4$ and $B_{2,5}$ conformers we next explored different mannosyl-configured donors, carrying different C6-modifications. We turned to rhamnose and mannuronic acid donors, in which the C6-CH_2OBn group of mannose is replaced by the slightly smaller and electronically different CH_3 or CO_2Me group, respectively. Mannuronic acid donors have been shown to provide 1,2-*cis* products with a wide variety of acceptors in a very reliable manner, and it has been reported that in the *C*-glycosylation reaction with allyltrimethylsilane solely the β-allyl products are obtained,[60] in contrast to their mannose counterparts.

Thus, we subjected the rhamnosyl and mannuronosyl donors, **15** and **16**, respectively, to the same set of model *C*-nucleophiles, as described above, to reveal the stereoselectivity trends shown in Table 2. We also performed the ASM/EDA

Table 2 Model *C*-glycosylation reaction results from mannosyl donor, **14**, rhamnosyl donor, **15**, and mannuronosyl donor, **16**. The stereoselectivity of the reaction is expressed as α : β and based on ^{1}H-NMR of purified α/β-product mixtures. Pre-activation-based glycosylation conditions were used: donor **14–16** (1.0 eq.), Tf_2O (1.3 eq.), Ph_2SO (1.3 eq.), TTBP (2.5 eq.), DCM (0.05 M), −80 to −60 °C, then add nucleophile (2.0 eq.) at −80 °C and allow to warm to −60 °C[1]

		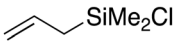 A	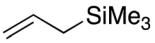 B	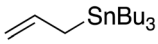 C
N		-0.45	1.79	4.41
Donor		α:β (yield)	α:β (yield)	α:β (yield)
14	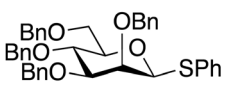	**14A** >98:2 (23%)	**14B** 72:28 (66%)	**14D** 28:72 (69%)
15	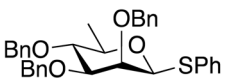	**15A** 89:11 (43%)	**15B** 50:50 (72%)	**15D** 25:75 (77%)
16	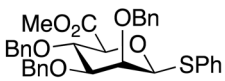	**16A** <2:98 (39%)	**16B** <2:98 (73%)	**16D** <2:98 (64%)

>90:10	>75:25	>60:40	50:50	<40:60	<25:75	<10:90

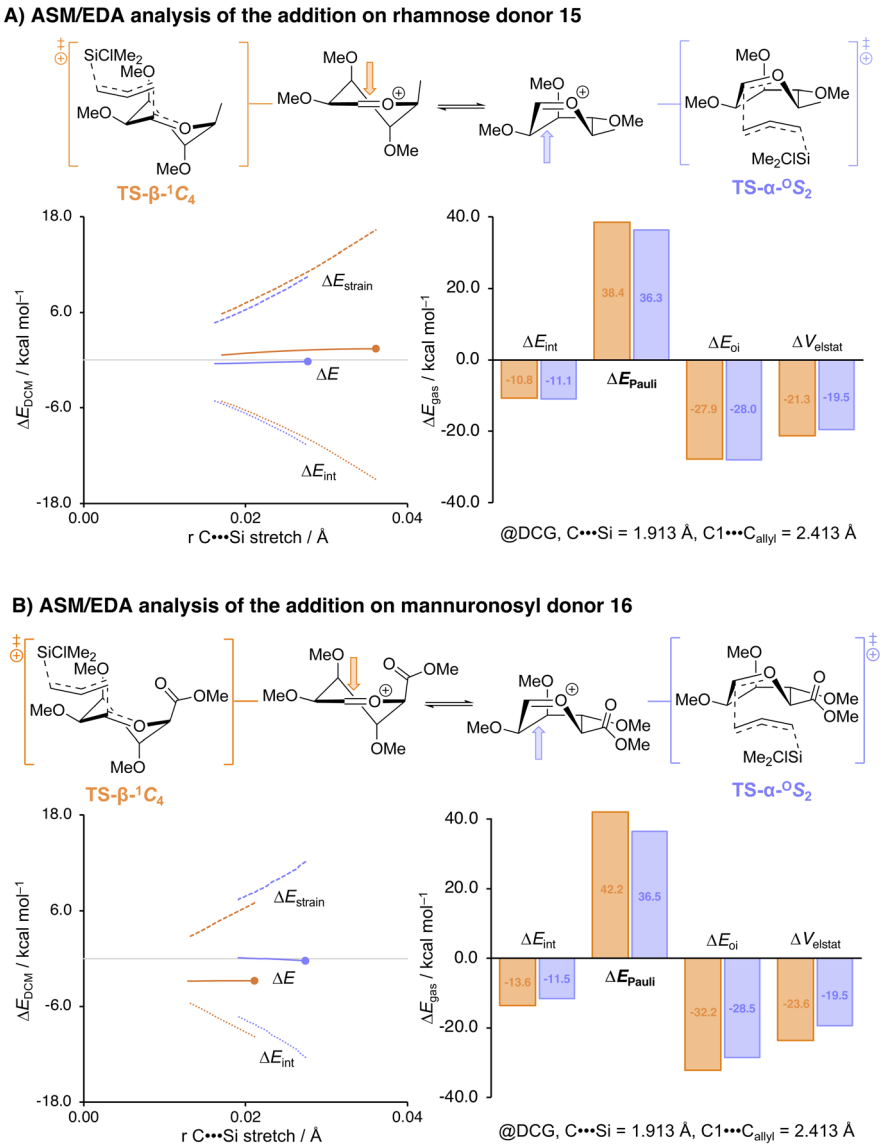

Fig. 4 Activation strain and energy decomposition analyses for the S_E2' reactions of allyl (chloro)dimethylsilane and the (A) rhamnosyl cation and (B) the mannuronosyl cation *via* the β-product-forming TS-β-$^1C_4$ (orange) and the α-product-forming TS-α-$^OS_2$ (light violet). Energy values are plotted to the transition state (indicated by a dot), along the IRC projected on the C···Si bond stretch. Energies are depicted as electronic energies and were computed at PCM(CH_2Cl_2)-B3LYP/6-311G (d,p) for ΔE_{DCM} or ZORA-B3LYP/TZ2P//PCM(CH_2Cl_2)-B3LYP/6-311G (d,p) for ΔE_{gas}.

analyses for the addition reactions for these donor systems. The profiles generated by these computational approaches are depicted in Fig. 4. Full potential energy profiles for the addition reactions to the rhamnosyl and mannuronosyl cations are provided in the SI (SI Fig. S3 and S4).

The rhamnose donor **15** displayed a reactivity-stereoselectivity trend that closely paralleled that of the mannosyl donor: across the series of allyl nucleophiles the product distribution shifted from the predominance of the α-product for the weakest nucleophile towards formation of more β-product with the stronger nucleophiles. The rhamnosylations were moderately but consistently more 1,2-*cis* selective than the mannosylations. The increase in the formation of the β-products can be rationalized by examining the ASM/EDA analyses. The reduced steric demand on the β-face delays the onset of Pauli repulsion and lowers its maximum along the β-$^1C_4$ trajectory, flattening the energy profiles and narrowing the energy difference between β- and α-attack (Fig. 4A). As a result, the kinetic advantage of the α-$^OS_2$ pathway is diminished, in comparison to the mannosylation reactions.

In sharp contrast to the reactions of the mannosyl and rhamnosyl donors, the mannuronic acid donor **16** furnished exclusively the β-products regardless of the reactivity of the used *C*-nucleophile. This behavior is consistent with an approach to the β-face of the most favorable $^3H_4$-like oxocarbenium ion and in line with the predictive two-conformer model. The persistence of β-selectivity with weak nucleophiles, where α-product formation could emerge through a Curtin–Hammett scenario,

can be attributed to the strong preference for the $^{3}H_4$ oxocarbenium ion conformer. This conformer is stabilized (with respect to the other conformers) by the carboxylate ester, which prefers to occupy a (pseudo)-axial orientation in an oxocarbenium ion species. When the ASM/EDA of the addition to the mannuronic acid ester ion is regarded, the effect of the carboxylic acid ester immediately becomes apparent (Fig. 4B); the β-$^{1}C_4$ pathway is associated with both significantly less strain than the α-$^{O}S_2$ itinerary and more stabilizing interaction energy. When the interaction energy is analyzed a trend similar to the mannosyl cation (Fig. 3A) is observed, the TS-α-$^{O}S_2$ pathway proceeds with significantly less Pauli repulsion and the β-$^{1}C_4$ pathway proceeds with more stabilizing electrostatic and orbital interactions. The difference in strain is already present at the start of the pathway, which can be traced back to the stability of the $^{3}H_4$ oxocarbenium ion. The high stability of this conformer raises the barrier to the formation of other conformers and prevents access to the $B_{2,5}$-$^{O}S_2$ pathway that is the dominant addition trajectory to the mannosyl ion.

Conclusions

This combined experimental and computational study establishes that the classical two-conformer model, while predictive for many glycosyl donors, does not adequately describe S_N1-type glycosylations of *manno*-configured donors. Detailed potential-energy surface mapping and activation-strain/energy-decomposition analyses reveal that attack of the mannosyl cation, leads to strong steric (Pauli) repulsion along the β-$^{1}C_4$ trajectory. The small ground-state energy difference between $^{3}H_4$ and $B_{2,5}$ conformers, allows an alternative pathway to become competitive: α-attack on a $B_{2,5}$-like cation that passes through an $^{O}S_2$ transition state. This route provides a lower overall barrier than the canonical chair-like β-attack and accounts for the α-selectivity observed with weak nucleophiles.

Modifications of C6 of the mannose donor confirm and quantify the roles of steric and conformational effects. Reducing steric demand by utilizing a C6-CH_3 group (as in rhamnose) lowers steric (Pauli) repulsion and pushes selectivity towards 'two-conformer behavior'. In contrast, stabilizing the $^{3}H_4$ conformation with a C5-CO_2CH_3 moiety (as in mannuronic acid) widens the energy gap between the $^{3}H_4$ and $B_{2,5}$ conformers, enforcing exclusive β-selectivity.

Together, these findings extend the mechanistic framework for S_N1-type glycosylations beyond the classical two-conformer model. They show that higher-energy boat-like intermediates can control stereochemistry when they offer a lower-repulsion reaction trajectory and that small, targeted changes in ring substitution can be used to bias glycosylation outcomes in a predictable way. This insight provides a quantitative foundation for designing stereoselective glycosylation reactions and highlights the need to critically (re-)examine other oxocarbenium ion conformers for different glycosyl configurations, as similarly unconventional boat-like or other high-energy intermediates may play underappreciated roles in determining selectivity.

Author contributions

JDCC, TH, FMB: conceptualisation; DH, WAR, JS: investigation; JDCC, TH, FMB: supervision; DH, WAR, JDCC: writing – original draft; DH, WAR, JS, FMB, TH, JDCC: writing – review & editing.

Conflicts of interest

There are no conflicts to declare.

Data availability

The data supporting this article have been included as part of the supplementary information (SI). Supplementary information is available. See DOI: https://doi.org/10.1039/d6sc02312f.

Acknowledgements

We thank the Netherlands Organization for Scientific Research (NWO) for financial support. Quantum chemical calculations were performed at the SURFsara HPC center in Amsterdam (2021/ENW/01070753, 2023/ENW/01446401 awarded to J. D. C. C). This research was supported by the Nederlandse Organisatie voor Wetenschappelijk Onderzoek (NWO-VICIVI.C.182.020, NWO-VIDIVI.C.182.020 to J. D. C. C.) and the European research Council (ERC-CoG-726072-"GLYCONTROL", to J. D. C. C.).

Notes and references

1 J. D. C. Codée, R. E. J. N. Litjens, R. den Heeten, H. S. Overkleeft, J. H. van Boom and G. A. van der Marel, Ph_2SO/Tf_2O: a Powerful Promotor System in Chemoselective Glycosylations Using Thioglycosides, *Org. Lett.*, 2003, **5**(9), 1519–1522, DOI: 10.1021/ol034312t.

2 The TS-α-$^{O}S_2$ transition states for both glycosyl cations could not be identified because these are not stationary points on the PES. Instead, a constrained potential energy surface was constructed by step-wise scanning the C···Nucleophile bond distance. As a representative structure for the transition state geometry, the point on the associated constrained potential energy surface with a similar C···Si bond stretch as the TS-α-$^{4}C_1$ was selected.

3 ASM calculations were performed in Gaussian 09, whereas EDA was carried out using the ADF 2018 module in the AMS program suite. Comparison of representative pathways confirms that interaction trends are invariant across methods.

4 P. O. Adero, H. Amarasekara, P. Wen, L. Bohé and D. Crich, The Experimental Evidence in Support of Glycosylation Mechanisms at the S_N1–S_N2 Interface, *Chem. Rev.*, 2018, **118**(17), 8242–8284, DOI: 10.1021/acs.chemrev.8b00083.

5 A. A. Hettikankanamalage, R. Lassfolk, F. S. Ekholm, R. Leino and D. Crich, Mechanisms of Stereodirecting Participation and Ester Migration from Near and Far in Glycosylation and Related Reactions, *Chem. Rev.*, 2020, **120**(15), 7104–7151, DOI: 10.1021/acs.chemrev.0c00243.

6 D. Crich, En Route to the Transformation of Glycoscience: A Chemist's Perspective on Internal and External Crossroads in Glycochemistry, *J. Am. Chem. Soc.*, 2021, **143**(1), 17–34, DOI: 10.1021/jacs.0c11106.

7 P. R. Andreana and D. Crich, Guidelines for *O*-Glycoside Formation from First Principles, *ACS Cent. Sci.*, 2021, **7**(9), 1454–1462, DOI: 10.1021/acscentsci.1c00594.

8 T. Hansen, S. van der Vorm, C. Tugny, W. A. Remmerswaal, J. M. A. van Hengst, G. A. van der Marel and J. D. C. Codée, Stereoelectronic Effects in Glycosylation Reactions, In *Comprehensive Glycoscience*, ed. J. J. Barchi, Elsevier, 2nd edn, 2021, pp. 83–102.

9 J. C. Kendale, E. M. Valentín and K. A. Woerpel, Solvent Effects in the Nucleophilic Substitutions of Tetrahydropyran Acetals Promoted by Trimethylsilyl Trifluoromethanesulfonate: Trichloroethylene as Solvent for Stereoselective *C*- and *O*-Glycosylations, *Org. Lett.*, 2014, **16**(14), 3684–3687, DOI: 10.1021/ol501471c.

10 J. R. Krumper, W. A. Salamant and K. A. Woerpel, Continuum of Mechanisms for Nucleophilic Substitutions of Cyclic Acetals, *Org. Lett.*, 2008, **10**(21), 4907–4910, DOI: 10.1021/ol8019956.

11 J. R. Krumper, W. A. Salamant and K. A. Woerpel, Correlations Between Nucleophilicities and Selectivities in the Substitutions of Tetrahydropyran Acetals, *J. Org. Chem.*, 2009, **74**(21), 8039–8050, DOI: 10.1021/jo901639b.

12 S. van der Vorm, T. Hansen, J. M. A. van Hengst, H. S. Overkleeft, G. A. van der Marel and J. D. C. Codée, Acceptor reactivity in glycosylation reactions, *Chem. Soc. Rev.*, 2019, **48**(17), 4688–4706, DOI: 10.1039/C8CS00369F.

13 S. van der Vorm, T. Hansen, H. S. Overkleeft, G. A. van der Marel and J. D. C. Codée, The influence of acceptor nucleophilicity on the glycosylation reaction mechanism, *Chem. Sci.*, 2017, **8**(3), 1867–1875, DOI: 10.1039/C6SC04638J.

14 C.-W. Chang, D. Wehner, G. R. D. Prabhu, E. Moon, M. Safferthal, L. Bechtella, N. Österlund, G. M. Vos and K. Pagel, Elucidating reactive sugar-intermediates by mass spectrometry, *Commun. Chem.*, 2025, **8**(1), 67, DOI: 10.1038/s42004-025-01467-5.

15 F. t. Braak, H. Elferink, K. J. Houthuijs, J. Oomens, J. Martens and T. J. Boltje, Characterization of Elusive Reaction Intermediates Using Infrared Ion Spectroscopy: Application to the Experimental Characterization of Glycosyl Cations, *Acc. Chem. Res.*, 2022, **55**(12), 1669–1679, DOI: 10.1021/acs.accounts.2c00040.

16 A. Franconetti, A. Ardá, J. L. Asensio, Y. Blériot, S. Thibaudeau and J. Jiménez-Barbero, Glycosyl Oxocarbenium Ions: Structure, Conformation, Reactivity, and Interactions, *Acc. Chem. Res.*, 2021, **54**(11), 2552–2564, DOI: 10.1021/acs.accounts.1c00021.

17 A. Martin, A. Arda, J. Désiré, A. Martin-Mingot, N. Probst, P. Sinaÿ, J. Jiménez-Barbero, S. Thibaudeau and Y. Blériot, Catching elusive glycosyl cations in a condensed phase with HF/SbF5 superacid, *Nat. Chem.*, 2016, **8**(2), 186–191, DOI: 10.1038/nchem.2399.

18 E. Mucha, M. Marianski, F.-F. Xu, D. A. Thomas, G. Meijer, G. von Helden, P. H. Seeberger and K. Pagel, Unravelling the structure of glycosyl cations via cold-ion infrared spectroscopy, *Nat. Commun.*, 2018, **9**(1), 4174, DOI: 10.1038/s41467-018-06764-3.

19 H. Elferink, M. E. Severijnen, J. Martens, R. A. Mensink, G. Berden, J. Oomens, F. P. J. T. Rutjes, A. M. Rijs and T. J. Boltje, Direct Experimental Characterization of Glycosyl Cations by Infrared Ion Spectroscopy, *J. Am. Chem. Soc.*, 2018, **140**(19), 6034–6038, DOI: 10.1021/jacs.8b01236.

20 M. Marianski, E. Mucha, K. Greis, S. Moon, A. Pardo, C. Kirschbaum, D. A. Thomas, G. Meijer, G. von Helden, K. Gilmore, *et al.*, Remote Participation during Glycosylation Reactions of Galactose Building Blocks: Direct Evidence from Cryogenic Vibrational Spectroscopy, *Angew. Chem., Int. Ed.*, 2020, **59**(15), 6166–6171, DOI: 10.1002/anie.201916245.

21 K. Greis, C. Kirschbaum, S. Leichnitz, S. Gewinner, W. Schöllkopf, G. von Helden, G. Meijer, P. H. Seeberger and K. Pagel, Direct Experimental Characterization of the Ferrier Glycosyl Cation in the Gas Phase, *Org. Lett.*, 2020, **22**(22), 8916–8919, DOI: 10.1021/acs.orglett.0c03301.

22 K. Greis, C. Kirschbaum, G. Fittolani, E. Mucha, R. Chang, G. von Helden, G. Meijer, M. Delbianco, P. H. Seeberger and K. Pagel, Neighboring Group Participation of Benzoyl Protecting Groups in C3- and C6-Fluorinated Glucose, *Eur. J. Org Chem.*, 2022, **2022**(15), e202200255, DOI: 10.1002/ejoc.202200255.

23 M. H. El-Badri, D. Willenbring, D. J. Tantillo and J. Gervay-Hague, Mechanistic Studies on the Stereoselective Formation of β-Mannosides from Mannosyl Iodides Using α-Deuterium Kinetic Isotope Effects, *J. Org. Chem.*, 2007, **72**(13), 4663–4672, DOI: 10.1021/jo070229y.

24 A. G. Santana, L. Montalvillo-Jiménez, L. Díaz-Casado, F. Corzana, P. Merino, F. J. Cañada, G. Jiménez-Osés, J. Jiménez-Barbero, A. M. Gómez and J. L. Asensio, Dissecting the Essential Role of Anomeric β-Triflates in Glycosylation Reactions, *J. Am. Chem. Soc.*, 2020, **142**(28), 12501–12514, DOI: 10.1021/jacs.0c05525.

25 D. Crich and N. S. Chandrasekera, Mechanism of 4,6-*O*-Benzylidene-Directed β-Mannosylation as Determined by α-Deuterium Kinetic Isotope Effects, *Angew. Chem., Int. Ed.*, 2004, **43**(40), 5386–5389, DOI: 10.1002/anie.200453688.

26 M. Huang, P. Retailleau, L. Bohé and D. Crich, Cation Clock Permits Distinction Between the Mechanisms of α- and β-*O*- and β-*C*-Glycosylation in the Mannopyranose Series: Evidence for the Existence of a Mannopyranosyl Oxocarbenium Ion, *J. Am. Chem. Soc.*, 2012, **134**(36), 14746–14749, DOI: 10.1021/ja307266n.

27 P. Merino, I. Delso, S. Pereira, S. Orta, M. Pedrón and T. Tejero, Computational evidence of glycosyl cations, *Org. Biomol. Chem.*, 2021, **19**(11), 2350–2365, DOI: 10.1039/D0OB02373F.

28 R. J. Woods, Computational carbohydrate chemistry: what theoretical methods can tell us, *Glycoconjugate J.*, 1998, **15**(3), 209–216, DOI: 10.1023/A:1006984709892.

29 R. J. Woods, C. W. Andrews and J. P. Bowen, Molecular mechanical investigations of the properties of oxocarbenium ions. 2. Application to glycoside hydrolysis,

J. Am. Chem. Soc., 1992, **114**(3), 859–864, DOI: 10.1021/ja00029a008.

30 A. Bérces, G. Enright, T. Nukada and D. M. Whitfield, The Conformational Origin of the Barrier to the Formation of Neighboring Group Assistance in Glycosylation Reactions: A Dynamical Density Functional Theory Study, *J. Am. Chem. Soc.*, 2001, **123**(23), 5460–5464, DOI: 10.1021/ja001194l.

31 D. M. Whitfield, DFT studies of the ionization of alpha and beta glycopyranosyl donors, *Carbohydr. Res.*, 2007, **342**(12), 1726–1740, DOI: 10.1016/j.carres.2007.05.012.

32 D. M. Whitfield, Plausible transition states for glycosylation reactions, *Carbohydr. Res.*, 2012, **356**, 180–190, DOI: 10.1016/j.carres.2012.03.040.

33 D. M. Whitfield, In a glycosylation reaction how does a hydroxylic nucleophile find the activated anomeric carbon?, *Carbohydr. Res.*, 2015, **403**, 69–89, DOI: 10.1016/j.carres.2014.05.021.

34 T. Hansen, L. Lebedel, W. A. Remmerswaal, S. van der Vorm, D. P. A. Wander, M. Somers, H. S. Overkleeft, D. V. Filippov, J. Désiré, A. Mingot, *et al.*, Defining the S_N1 Side of Glycosylation Reactions: Stereoselectivity of Glycopyranosyl Cations, *ACS Cent. Sci.*, 2019, **5**(5), 781–788, DOI: 10.1021/acscentsci.9b00042.

35 Y. Chun, K. B. Luu and K. A. Woerpel, Acetal Substitution Reactions: Stereoelectronic Effects, Conformational Analysis, Reactivity vs. Selectivity, and Neighboring-Group Participation, *Synlett*, 2024, **35**(15), 1763–1787, DOI: 10.1055/s-0042-1751541.

36 T. Nukada, A. Bérces, L. Wang, M. Z. Zgierski and D. M. Whitfield, The two-conformer hypothesis: 2,3,4,6-tetra-*O*-methyl-mannopyranosyl and -glucopyranosyl oxacarbenium ions, *Carbohydr. Res.*, 2005, **340**(5), 841–852, DOI: 10.1016/j.carres.2004.12.021.

37 A. Fürst and P. A. Plattner, Über Steroide und Sexualhormone. 160. Mitteilung. 2*α*, 3*α*- und 2β, 3β-Oxidochlolestane; Konfiguration der 2-Oxy-cholestane, *Helv. Chim. Acta*, 1949, **32**(1), 275–283, DOI: 10.1002/hlca.19490320139.

38 M. Miljković, D. Yeagley, P. Deslongchamps and Y. L. Dory, Experimental and Theoretical Evidence of Through-Space Electrostatic Stabilization of the Incipient Oxocarbenium Ion by an Axially Oriented Electronegative Substituent During Glycopyranoside Acetolysis, *J. Org. Chem.*, 1997, **62**(22), 7597–7604, DOI: 10.1021/jo970677d.

39 M. T. Yang and K. A. Woerpel, The Effect of Electrostatic Interactions on Conformational Equilibria of Multiply Substituted Tetrahydropyran Oxocarbenium Ions, *J. Org. Chem.*, 2009, **74**(2), 545–553, DOI: 10.1021/jo8017846.

40 M. G. Beaver and K. A. Woerpel, Erosion of Stereochemical Control with Increasing Nucleophilicity: O-Glycosylation at the Diffusion Limit, *J. Org. Chem.*, 2010, **75**(4), 1107–1118, DOI: 10.1021/jo902222a.

41 S. B. Billings and K. A. Woerpel, Nucleophilic Substitution Reactions of Sulfur-Substituted Cyclohexanone Acetals: An Analysis of the Factors Controlling Stereoselectivity, *J. Org. Chem.*, 2006, **71**(14), 5171–5178, DOI: 10.1021/jo060077r.

42 J. A. C. Romero, S. A. Tabacco and K. A. Woerpel, Stereochemical Reversal of Nucleophilic Substitution Reactions Depending upon Substituent: Reactions of Heteroatom-Substituted Six-Membered-Ring Oxocarbenium Ions through Pseudoaxial Conformers, *J. Am. Chem. Soc.*, 2000, **122**(1), 168–169, DOI: 10.1021/ja993366o.

43 S. Chamberland, J. W. Ziller and K. A. Woerpel, Structural Evidence that Alkoxy Substituents Adopt Electronically Preferred Pseudoaxial Orientations in Six-Membered Ring Dioxocarbenium Ions, *J. Am. Chem. Soc.*, 2005, **127**(15), 5322–5323, DOI: 10.1021/ja050830i.

44 L. Ayala, C. G. Lucero, J. A. C. Romero, S. A. Tabacco and K. A. Woerpel, Stereochemistry of Nucleophilic Substitution Reactions Depending upon Substituent: Evidence for Electrostatic Stabilization of Pseudoaxial Conformers of Oxocarbenium Ions by Heteroatom Substituents, *J. Am. Chem. Soc.*, 2003, **125**(50), 15521–15528, DOI: 10.1021/ja037935a.

45 C. G. Lucero and K. A. Woerpel, Stereoselective C-Glycosylation Reactions of Pyranoses: The Conformational Preference and Reactions of the Mannosyl Cation, *J. Org. Chem.*, 2006, **71**(7), 2641–2647, DOI: 10.1021/jo0522963.

46 K. M. Demkiw, W. A. Remmerswaal, T. Hansen, G. A. van der Marel, J. D. C. Codee and K. A. Woerpel, Halogen Atom Participation in Guiding the Stereochemical Outcomes of Acetal Substitution Reactions, *Angew Chem. Int. Ed. Engl.*, 2022, **61**(42), e202209401, DOI: 10.1002/anie.202209401.

47 W. A. Remmerswaal, T. Hansen, T. A. Hamlin and J. D. C. Codee, Origin of Stereoselectivity in S_E2' Reactions of Six-membered Ring Oxocarbenium Ions, *Chemistry*, 2023, **29**(14), e202203490, DOI: 10.1002/chem.202203490.

48 G. Hagen and H. Mayr, Kinetics of the reactions of allylsilanes, allylgermanes, and allylstannanes with carbenium ions, *J. Am. Chem. Soc.*, 1991, **113**(13), 4954–4961, DOI: 10.1021/ja00013a035.

49 H. Mayr, T. Bug, M. F. Gotta, N. Hering, B. Irrgang, B. Janker, B. Kempf, R. Loos, A. R. Ofial, G. Remennikov, *et al.*, Reference Scales for the Characterization of Cationic Electrophiles and Neutral Nucleophiles, *J. Am. Chem. Soc.*, 2001, **123**(39), 9500–9512, DOI: 10.1021/ja010890y.

50 H. Mayr, B. Kempf and A. R. Ofial, π-Nucleophilicity in Carbon−Carbon Bond-Forming Reactions, *Acc. Chem. Res.*, 2003, **36**(1), 66–77, DOI: 10.1021/ar020094c.

51 D. Crich and I. Sharma, Is Donor−Acceptor Hydrogen Bonding Necessary for 4,6-*O*-Benzylidene-directed β-Mannopyranosylation? Stereoselective Synthesis of β-*C*-Mannopyranosides and α-C-Glucopyranosides, *Org. Lett.*, 2008, **10**(21), 4731–4734, DOI: 10.1021/ol8017038.

52 G. J. McGarvey, C. A. LeClair and B. A. Schmidtmann, Studies on the Stereoselective Synthesis of *C*-Allyl Glycosides, *Org. Lett.*, 2008, **10**(21), 4727–4730, DOI: 10.1021/ol801710s.

53 F. M. Bickelhaupt and K. N. Houk, Analyzing Reaction Rates with the Distortion/Interaction-Activation Strain Model, *Angew. Chem., Int. Ed.*, 2017, **56**(34), 10070–10086, DOI: 10.1002/anie.201701486.

54 F. M. Bickelhaupt, Understanding reactivity with Kohn–Sham molecular orbital theory: E2–S_N2 mechanistic

spectrum and other concepts, *J. Comput. Chem.*, 1999, **20**(1), 114–128, DOI: 10.1002/(SICI)1096-987X(19990115)20:1<114::AID-JCC12>3.0.CO;2-L.

55 T. Hansen, X. Sun, M. Dalla Tiezza, W.-J. van Zeist, J. N. P. van Stralen, D. P. Geerke, L. P. Wolters, J. Poater, T. A. Hamlin and F. M. Bickelhaupt, C–X Bond Activation by Palladium: Steric Shielding versus Steric Attraction, *Chem. - Eur. J.*, 2022, **28**(44), e202201093, DOI: 10.1002/chem.202201093.

56 T. Hansen, P. Vermeeren, A. Haim, M. J. H. van Dorp, J. D. C. Codée, F. M. Bickelhaupt and T. A. Hamlin, Regioselectivity of Epoxide Ring-Openings via S_N2 Reactions Under Basic and Acidic Conditions, *Eur. J. Org Chem.*, 2020, **2020**(25), 3822–3828, DOI: 10.1002/ejoc.202000590.

57 Implicit solvation (PCM(CH_2Cl_2)) was found to uniformly stabilize the reacting species without affecting the relative ordering of the pathways. Consequently, the trends obtained from gas-phase EDA are representative of those under solvated conditions.

58 E. Blokker, X. Sun, J. Poater, J. M. van der Schuur, T. A. Hamlin and F. M. Bickelhaupt, The Chemical Bond: When Atom Size Instead of Electronegativity Difference Determines Trend in Bond Strength, *Chem. - Eur. J.*, 2021, **27**(63), 15616–15622, DOI: 10.1002/chem.202103544.

59 D. Rodrigues Silva, E. Blokker, J. M. van der Schuur, T. A. Hamlin and F. M. Bickelhaupt, Nature and strength of group-14 A–A′ bonds, *Chem. Sci.*, 2024, **15**(5), 1648–1656, DOI: 10.1039/D3SC06215E.

60 J. D. C. Codée, L. J. van den Bos, A.-R. de Jong, J. Dinkelaar, G. Lodder, H. S. Overkleeft and G. A. van der Marel, The Stereodirecting Effect of the Glycosyl C5-Carboxylate Ester: Stereoselective Synthesis of β-Mannuronic Acid Alginates, *J. Org. Chem.*, 2009, **74**(1), 38–47, DOI: 10.1021/jo8020192.